Constraining the Jet Launching Time of GRB 170817A by Utilizing the Baryon Loading

Jia Ren , Da-Bin Lin , Lu-Lu Zhang , Kai Wang, Xiao-Yan Li, Xiang-Gao Wang , and En-Wei Liang
Laboratory for Relativistic Astrophysics, Department of Physics, Guangxi University, Nanning 530004, People's Republic of China; lindabin@gxu.edu.cn

Abstract

The observed delay of GRB 170817A relative to GW170817 provides significant information about gamma-ray burst (GRB) physics, and is subject to intense debate. In this Letter, we present an approach for discussing the major source of this time delay. First, we use the structured jet model to fit the X-ray/optical/radio afterglows of GRB 170817A together with superluminal motion measured using Very Long Baseline Interferometry. Our structured jet is modeled with angle-dependent energy and baryon loading. It is found that our model well fits the afterglows of GRB 170817A. Then, the baryon loading in the jet is inferred based on our fitting results. By comparing the baryon loading to the mass outflow in different stages, we infer that the time lag of the jet launch relative to the merger is less than hundreds or tens of milliseconds. It suggests that the time delay of GRB 170817A relative to GW170817 is defined mostly by the spreading time of the jet propagating to its dissipation radius.

1. Introduction

On 2017 August 17 at 12:41:04 UTC, the Advanced Laser Interferometer Gravitational-wave Observatory and the Advanced Virgo gravitational-wave detectors made their first observation of a gravitational wave (GW) event, GW170817, from a binary neutron star (NS) merger (Abbott et al. 2017a, 2017c, 2017d, 2017e). GW170817 was followed by a short gamma-ray burst (GRB), GRB 170817A (Abbott et al. 2017b; Goldstein et al. 2017; Zhang et al. 2018), which triggered the Fermi Gamma-ray Burst Monitor at $t_{\rm obs} \sim 1.7$ s after the GW signal and lasted for ~ 2 s. The delay of GRB 170817A relative to GW170817 is a subject of intense debate in the field of GRBs (Zhang 2018, 2019; Burns 2019). With the exception of GRB 170817A, recent controversial gamma-ray signals, GBM-150914 (Connaughton et al. 2016, 2018; Greiner et al. 2016) and GBM-190816 (Yang et al. 2020), were claimed to follow the black hole–black hole (BH–BH) or BH–NS merger GW signals, GW150914 and GW190816, with a lag of ~ 0.4 s and ~ 1.57 s, respectively. It indicates that the time delay of a GRB relative to a GW signal may be common in compact binary mergers. There are two main arguments regarding the origin of the time delay for a GRB with respect to the GW signal. Some authors (e.g., Bromberg et al. 2018; Gottlieb et al. 2018) have attributed it to the co-effect of the delayed jet launching and the jet breakout from the ejecta. Other authors (e.g., Lin et al. 2018; Zhang et al. 2018) have suggested that the jet may be launched promptly after the merger, and that the delay is mostly defined by the spreading time when the jet propagates to the dissipation radius. However, to date there is no consensus.

Binary NS mergers are expected to release an amount of neutron-rich matter (Lattimer & Schramm 1974, 1976; Symbalisty & Schramm 1982), which can synthesize elements that are heavier than iron via the rapid neutron-capture process (*r*-process). Numerical simulations of NS–NS mergers reveal that a substantial amount of matter outflows from the system (see Nakar 2019 for a detailed introduction); e.g., the dynamic ejecta is formed in the first ~ 10 ms after the merger, the neutrino-driven wind is stripped from the accretion disk and central object, or the viscosity-driven wind is blown off by the disk heating. (Hereafter,

dynamic ejecta, neutrino-driven wind, and viscosity-driven wind are all referred to as "outflow" in order to distinguish it from the ultra-relativistic jet.) Owing to nucleosynthesis, there are many radioactive heavy elements in the outflowing material. Consequently, a kilonova powered by the radioactive decay of heavy elements will appear (Li & Paczyński 1998; also see Metzger 2017 for a review), e.g., AT2017gfo (Coulter et al. 2017). In different post-merger stages, the outflow has different properties, e.g., mass, angular distribution, and electron abundance, all of which affect the outcomes of synthesized elements. Thus, a "red," "blue," and even "purple" component emerges in kilonova observations (e.g., Villar et al. 2017; Zhu et al. 2020). Based on this multi-component prescription, many authors have presented their estimation on the ejecta properties by modeling and fitting AT2017gfo (e.g., Cowperthwaite et al. 2017; Kasen et al. 2017; Villar et al. 2017; Waxman et al. 2018). Furthermore, the possible effect of the compact remnant on AT2017gfo has been also studied (e.g., Li et al. 2018; Matsumoto et al. 2018; Yu et al. 2018; Ren et al. 2019). It is suggested that the compact remnant at least survived as an NS for some time, and thereby blown out enough material to power AT2017gfo (e.g., Metzger et al. 2018).

When an energetic jet expands outward, it is inevitably contaminated by baryons in the outflow. Thus, we propose the following. With a relatively detailed understanding of the spatial and temporal distribution of the merger outflows, it is possible to infer the waiting time of jet launching by comparing the baryon loading of the jet with the outflows in different post-merger stages. In this Letter, we perform the fitting of the GRB 170817A afterglow to infer the baryon loading of the jet in GRB 170817A and examine the jet launching time. This Letter is organized as follows. In Section 2, we introduce the models and methods used in our fitting. In Section 3, we give the fitting result and the corresponding discussion. The summary is made in Section 4.

2. Model and Superluminal Motion

To describe the jet structure and the dynamics of the external-forward shock, we introduce a spherical coordinate (r, θ, φ) with $r = 0$ located at the burst's central engine and

$\theta = 0$ along the jet axis. We assume the observer location at the direction of (θ_v, φ_v) with $\varphi_v = 0$.

Structured jet Description: In contrast to previous works, the structured jet is modeled with the angle-dependent baryon loading $\rho(\theta)$ and kinetic energy $\varepsilon(\theta)$ per solid angle in this work. We consider an axisymmetric power-law structured jet, i.e.,

$$E_{\rm iso}(\theta) = E_{\rm iso,0}\left(1 + \frac{\theta}{\theta_\varepsilon}\right)^k, \tag{1}$$

$$M_{\rm iso}(\theta) = M_{\rm iso,0}\left(1 + \frac{\theta}{\theta_\rho}\right)^s, \tag{2}$$

and an axisymmetric Gaussian structured jet, i.e.,

$$E_{\rm iso}(\theta) = E_{\rm iso,0}\exp\left(-\frac{\theta^2}{2\theta_\varepsilon^2}\right), \tag{3}$$

$$M_{\rm iso}(\theta) = M_{\rm iso,0}\exp\left(-\frac{\theta^2}{2\theta_\rho^2}\right), \tag{4}$$

where $E_{\rm iso}(\theta) = 4\pi\varepsilon(\theta)$, $M_{\rm iso}(\theta) = 4\pi\rho(\theta)$, and θ_ε and θ_ρ are the characteristic half opening angle of $\varepsilon(\theta)$ and $\rho(\theta)$, respectively.

Dynamics of the external-forward shock: The hemisphere that is centered in the jet axis is divided into 400×100 small patches along the θ and φ directions in their linear space. In this work, we assume that the jet has no lateral expansion (but see Troja et al. 2019), and that the dynamics of the external-forward shock is estimated independently in each patch, i.e., (Zhang 2018),

$$\frac{d\Gamma}{dr} = -\frac{\Gamma(\Gamma^2 - 1)(\hat{\gamma}\Gamma - \hat{\gamma} + 1)\frac{dm}{dr}c^2 - (\hat{\gamma} - 1)\Gamma(\hat{\gamma}\Gamma^2 - \hat{\gamma} + 1)(3U/r)}{\Gamma^2[\rho(\theta) + m]c^2 + (\hat{\gamma}^2\Gamma^2 - \hat{\gamma}^2 + 3\hat{\gamma} - 2)U}, \tag{5}$$

$$\frac{dU}{dr} = (1 - \epsilon)(\Gamma - 1)c^2\frac{dm}{dr} - (\hat{\gamma} - 1)\left(\frac{3}{r} - \frac{1}{\Gamma}\frac{d\Gamma}{dr}\right)U, \tag{6}$$

where $dm/dr = n_{\rm ISM}m_p r^2$ with $n_{\rm ISM}$ being the particle density of the interstellar medium (ISM), m_p being the proton mass, and $\Gamma(\theta, r)$, $m(\theta, r)$, $U(\theta, r)$, and ϵ being the bulk Lorentz factor, the sweep-up mass per solid angle, the internal energy, and the radiation efficiency of electrons in the external-forward shock, respectively. The adiabatic index is $\hat{\gamma} \simeq (5 - 1.21937\zeta + 0.18203\zeta^2 - 0.96583\zeta^3 + 2.32513\zeta^4 - 2.39332\zeta^5 + 1.07136\zeta^6)/3$ with $\zeta \equiv \Theta/(0.24 + \Theta)$, $\Theta \simeq \left(\frac{\Gamma\beta}{3}\right)\left[\frac{\Gamma\beta + 1.07(\Gamma\beta)^2}{1 + \Gamma\beta + 1.07(\Gamma\beta)^2}\right]$, and $\beta = \sqrt{1 - 1/\Gamma^2}$ (Pe'er 2012). The initial Lorentz factor of the patch is set as $\Gamma_0(\theta) = E_{\rm iso}(\theta)/[M_{\rm iso}(\theta)c^2] + 1$. Given an appropriate initial value of U, the r-dependent Γ can be obtained for each patch. The patches with $\Gamma_0(\theta) < 1.4$ are neglected in our calculations and not involved in the estimation of baryon loading. ϵ_e and ϵ_B are introduced to represent the fractions of the shock energy used to accelerate electrons and contributing to the

magnetic energy, respectively. Then, the magnetic field behind the shock is $B' = (32\pi\epsilon_B n_{\rm ISM})^{1/2}\Gamma c$. The sweep-up electrons are accelerated to a power-law distribution of Lorentz factor γ_e, i.e., $Q \propto \gamma_e'^{-p}$ for $\gamma_{e,\min}' \leqslant \gamma_e \leqslant \gamma_{e,\max}'$, where $p(>2)$ is the power-law index, $\gamma_{e,\min} = \epsilon_e(p - 2)m_p\Gamma/[(p - 1)m_e]$ (Sari et al. 1998), and $\gamma_{e,\max} = \sqrt{9m_e^2 c^4/(8B'q_e^3)}$ with q_e is the electron charge (e.g., Kumar et al. 2012). Then, one can have $\epsilon = \epsilon_{\rm rad}\epsilon_e$ with $\epsilon_{\rm rad} = \min\{1, (\gamma_{e,\min}/\gamma_{e,c})^{(p-2)}\}$ (Fan & Piran 2006), where $\gamma_{e,c} = 6\pi m_e c/(\sigma_{\rm T}\Gamma B'^2 t')$ is the efficient cooling Lorentz factor of electrons.

In the X-ray/optical/radio bands, the main radiation mechanism of the external-forward shock in GRBs is the synchrotron radiation of the sweep-up electrons (Sari et al. 1998; Sari & Piran 1999). We denote the instantaneous electron spectrum per solid angle at r and θ as $n_e'(r, \theta, \gamma_e')$, of which the evolution can be solved based on the continuity equation (e.g., Liu et al. 2020). The spectral power of synchrotron radiation of $n_e'(r, \theta, \gamma_e')$ at a given frequency ν' is

$P'(\nu', r, \theta) = \frac{\sqrt{3}q_e^3 B'}{m_e c^2}\int_0^{\gamma'_{\max}} F(\nu'/\nu_c')n_e'd\gamma_e'$, where $F(x) = x\int_x^{+\infty} K_{5/3}(k)dk$ with $K_{5/3}(k)$ being the modified Bessel function of 5/3 order and $\nu_c' = 3q_e B'\gamma_e'^2/(4\pi m_e c)$. By summing the flux from each patch observed at a same observer time $t_{\rm obs}$, the total observed flux can be obtained.

Superluminal Motion of Flux Centroid: The flux centroid motion, as well as the axial ratio of the image, are powerful tools to constrain the jet structure (Gill & Granot 2018). In our calculations, we record the location $(x, y, z) = (r\sin\theta\cos\varphi,\ r\sin\theta\sin\varphi,\ r\cos\theta)$ of the maximum flux in the radio image at 3 GHz band and the observer time $t_{\rm obs}$. Then, the apparent velocity of the flux centroid over a time interval $\delta t_{\rm obs} = t_{\rm obs,2} - t_{\rm obs,1}$ is estimated as

$\beta_{\rm app} \equiv v_{\rm app}/c = \sqrt{(x_2' - x_1')^2 + (y_2' - y_1')^2}/(\delta t_{\rm obs}c)$, where $x' = x\cos\theta_v - z\sin\theta_v$, $y' = y$, and (x_1, y_1, z_1) and (x_2, y_2, z_2) correspond to the observer time $t_{\rm obs,1}$ and $t_{\rm obs,2}$, respectively. It should be pointed out that an elliptical Gaussian fitting of the radio image should be performed in order to better estimate the location of flux centroid (e.g., Granot et al. 2018; Lu et al. 2020). However, our approach based on the location of maximum flux would significantly reduce the computation time.

3. Fitting Result and Discussion

3.1. Fitting on the Afterglows of GRB 170817A

The X-ray/optical/radio afterglows of GRB 170817A is fitted with our structured jet. Owing to the different process of data processing, the data from different groups may exhibit a lack of uniformity. Recently, Makhathini et al. (2020) compiled and unified all of the observational data about the afterglows of GRB 170817A. We take their result at 1 keV, F606W, 6 GHz, and 3 GHz bands as our fitting data set, which are shown in Figure 1. In addition, the superluminal motion $\beta_{\rm app} = 4.1 \pm 0.5$ between 75 and 230 days is also used in our fittings (Mooley et al. 2018). Our work includes the fitting with power-law and Gaussian structured jet models. The fitting is performed based on the Markov Chain Monte Carlo (MCMC) method to produce
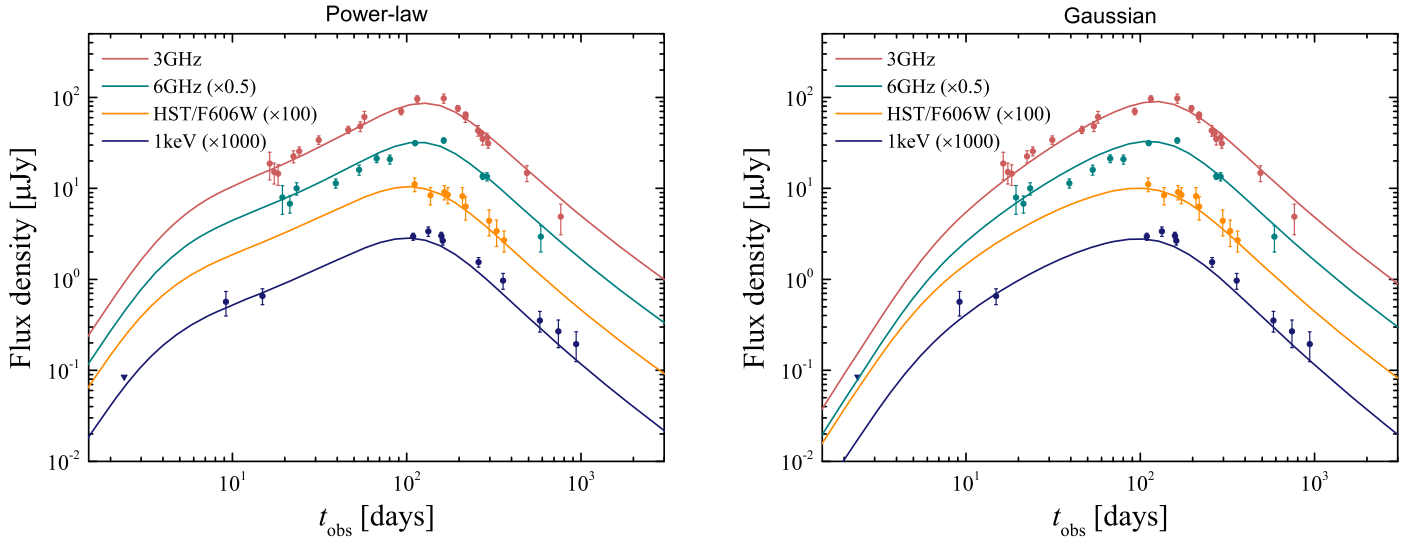
Figure 1. Fitting result (solid lines) of afterglows in GRB 170817A. The observational data are described with circles, where the triangle is the upper limit of X-ray.
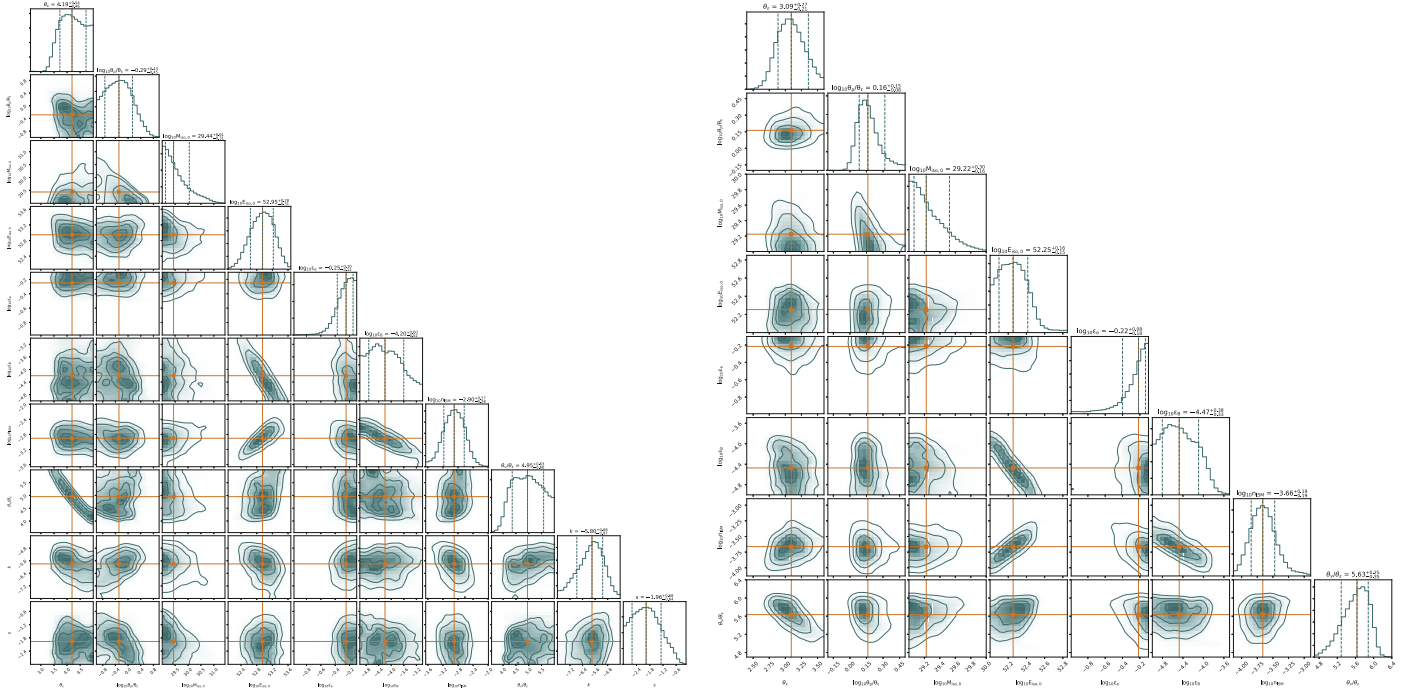
Figure 2. Corner plot for the power-law (left) and the Gaussian (right) structured jet model fitting to the afterglows of GRB 170817A.

posterior predictions for the model parameters. The Python package emcee (Foreman-Mackey et al. 2013) is used for our MCMC sampling, where $N_{\rm walkers} \times N_{\rm steps} = 25 \times 2000$ is adopted and the initial 10% iterations are used for burn-in. The projections of the posterior distribution in 1D and 2D for the physical parameters in the power-law model (i.e., $E_{\rm iso,0}$, $M_{\rm iso,0}$, ϵ_e, ϵ_B, $n_{\rm ISM}$, θ_ε, $\theta_\rho/\theta_\varepsilon$, $\theta_v/\theta_\varepsilon$, k, s) and the Gaussian model (i.e., $E_{\rm iso,0}$, $M_{\rm iso,0}$, ϵ_e, ϵ_B, $n_{\rm ISM}$, θ_ε, $\theta_\rho/\theta_\varepsilon$, $\theta_v/\theta_\varepsilon$) are presented in Figure 2. In this work, $p = 2.16$ is adopted by considering the spectrum fitting results (e.g., Fong et al. 2019). The obtained parameters at the 1σ confidence level are reported in Table 1, and the optimal fitting results are shown in Figure 1.

Note that recent works (e.g., Beniamini et al. 2020b; Nakar & Piran 2020; Ryan et al. 2020) have pointed out the wide range of θ_ε and θ_v values obtained from afterglow fittings is due to the lack of key information for fitting. Beniamini et al. (2020b) and

Nakar & Piran (2020) clearly indicate that the ratio $\theta_v/\theta_\varepsilon$ is the only quantity that can be determined from the light curve alone. Here, we use this ratio as one of the free parameters and find that $\theta_v/\theta_\varepsilon$ has a value $\sim$5 with maximum likelihood under the power-law structured jet model, which is in agreement with those works combined with the Very Long Baseline Interferometry (VLBI) superluminal measurement in the fittings (Ghirlanda et al. 2019; Hotokezaka et al. 2019). The degeneracy between θ_ε and $\theta_v/\theta_\varepsilon$ in Figure 2 suggests that the viewing angle θ_v can be robustly estimated from our fittings. Our obtained θ_ε and θ_v are consistent with the results estimated based on the prompt emission of GRB 170817 (e.g., Mooley et al. 2018; Beniamini et al. 2019). The ISM number density is well below the upper limit on the density of ionized and neutral particle density (e.g., Hallinan et al. 2017; Hajela et al. 2019). The small allowed spread in ϵ_e is consistent with the results of Beniamini & van der Horst (2017).

Table 1
Parameters Estimated from the MCMC Sampling

Parameter[a]	Power-law	Gaussian	Range
$\log_{10} E_{\mathrm{iso},0}$ (erg)	$52.95^{+0.28}_{-0.31}$	$52.25^{+0.16}_{-0.15}$	[52, 54]
$\log_{10} M_{\mathrm{iso},0}$ (g)	$29.44^{+0.61}_{-0.31}$	$29.22^{+0.30}_{-0.16}$	[29, 32]
$\log_{10} \epsilon_e$	$-0.25^{+0.10}_{-0.12}$	$-0.22^{+0.08}_{-0.18}$	[−2, −0.1]
$\log_{10} \epsilon_B$	$-4.20^{+0.60}_{-0.52}$	$-4.47^{+0.38}_{-0.33}$	[−5, −3]
$\log_{10} n_{\mathrm{ISM}}$ (cm^{-3})	$-2.90^{+0.27}_{-0.28}$	$-3.66^{+0.19}_{-0.19}$	[−5, −1]
θ_ε (°)	$4.19^{+0.54}_{-0.46}$	$3.09^{+0.27}_{-0.21}$	[2, 5]
$\log_{10} \theta_\rho / \theta_\varepsilon$	$-0.29^{+0.43}_{-0.45}$	$0.16^{+0.15}_{-0.08}$	[−1, 1]
$\theta_v / \theta_\varepsilon$	$4.95^{+0.63}_{-0.60}$	$5.63^{+0.25}_{-0.35}$	[2, 6]
k	$-5.80^{+0.68}_{-0.97}$	⋯	[−8, −3]
s	$-1.96^{+0.68}_{-0.64}$	⋯	[−3, −0.1]
p	2.16	2.16	frozen
θ_v (°)	$20.65^{+0.66}_{-0.66}$	$17.36^{+0.87}_{-0.83}$	⋯
M_{jet} ($M_\odot$)	$2.49^{+1.44}_{-1.30} \times 10^{-7}$	$3.16^{+2.04}_{-1.23} \times 10^{-7}$	⋯
E_{jet} (erg)	$1.25^{+0.97}_{-0.56} \times 10^{49}$	$2.71^{+1.28}_{-0.90} \times 10^{49}$	⋯

Note.
[a] There are strong degeneracies between $E_{\mathrm{iso},0}$, ϵ_B, and n_{ISM}, as shown in Figure 2. It reveals that a series of parameter sets could fit the afterglows of GRB 170817A and the values very far from the estimated median value may be possible. In addition, the value of θ_v, M_{jet}, and E_{jet} are estimated based on the MCMC samples rather than the estimated median values.

For our power-law structured jet, the value of $k \sim -6$ and $s \sim -2$ means $\Gamma(\theta) \propto \theta^{-4}$ at large angle. This is consistent with that found in Ghirlanda et al. (2019), of which $E(\theta) \propto \theta^{-5.5}$ and $\Gamma(\theta) \propto \theta^{-3.5}$ is found. Hotokezaka et al. (2019) found $E(\theta) \propto \theta^{-4.5}$ and $\Gamma(\theta) \propto \theta^{-4.5}$ by freezing the value of $\Gamma(\theta = 0) = 600$. Based on our optimal fitting result, $\Gamma(\theta = 0) = 360$ rather than 600 is obtained. Then, the low value of the power-law index in the $\theta-\Gamma$ relation found in Hotokezaka et al. (2019) may be the result of the high value of $\Gamma(\theta = 0)$ adopted in their fittings.

In Figure 3, we show the evolution of the apparent velocity β_{app} of flux centroid motion at 3 GHz band based on our optimal fitting result of the power-law model, where the time interval of 10 days is adopted. For comparison, we also show other noteworthy parameters in this figure: ① Γ_{axis}, the bulk Lorentz factor of the jet flow along the jet axis; ② Γ_{fc}, the bulk Lorentz factor of flux centroid; ③ $\beta_{\mathrm{app,axis}} = \beta_{\mathrm{axis}} \sin \theta_v / (1 - \beta_{\mathrm{axis}} \cos \theta_v)$ and $\beta_{\mathrm{app,fc}} = \beta_{\mathrm{fc}} \sin \alpha_{\mathrm{fc}} / (1 - \beta_{\mathrm{fc}} \cos \alpha_{\mathrm{fc}})$, where $\beta_{\mathrm{axis}} = (1 - \Gamma_{\mathrm{axis}}^{-2})^{1/2}$, $\beta_{\mathrm{fc}} = (1 - \Gamma_{\mathrm{fc}}^{-2})^{1/2}$, and α_{fc} is the angle between the flux centroid and the line of sight (Rees 1966). In the inset of this figure, we zoom in the figure for the details in the period of $t_{\mathrm{obs}} \sim [70, 300]$ days. One can find that Γ_{fc} is almost a constant during the early phase ($t_{\mathrm{obs}} \lesssim 160$ days), which corresponds to the rising phase of afterglows. It indicates that the flux centroid tracks a region that has a specific bulk Lorentz factor in this phase. At the early stage, β_{app} is always larger than $\beta_{\mathrm{app,fc}}$, which stems from the movement of the flux centroid region in the θ-direction from $\theta \sim \theta_v$ to $\theta = 0$. The discrepancy of β_{app} with $\beta_{\mathrm{app,fc}}$ and $\beta_{\mathrm{app,axis}}$ reminds that the apparent velocity of a structured jet should be well estimated in the fittings of its afterglows.

3.2. Baryon Loading and Constraining on the Jet Launching Time

According to the MCMC samples, the baryon loading of the jet M_{jet} can be estimated, and its distribution is shown in the right panel of Figure 4. In this panel, the red and blue histograms correspond to those from the power-law and Gaussian structured jets, respectively. Then, $M_{\mathrm{jet}} = 2.49^{+1.44}_{-1.30} \times 10^{-7} M_\odot$ and $M_{\mathrm{jet}} = 3.16^{+2.04}_{-1.23} \times 10^{-7} M_\odot$ are obtained for the power-law and Gaussian structured jets, respectively. The median value and 1σ uncertainty of M_{jet}, respectively, are also shown with dashed–dotted lines and filled regions in the left panel with the same color in the right panel.

In this subsection, the obtained M_{jet} is used to constrain the jet launching time by considering the time/angle-dependent outflow in different ejecting stages. We assume that when a jet propagates in the surrounding outflowing material, a fraction η of the material in the path of its propagation is drawn into the jet and becomes a part of M_{jet}. Recent works that focus on the interaction of a jet with its surrounding outflow show that the structure of jet depends strongly on the mixing taking place both inside the cocoon and along the jet-cocoon interface. The degree of the mixing would strongly affect the value of η. Gottlieb et al. (2020a, 2020b) reveal that the jet power, the angle of the initial injected jet, and the medium density can strongly influence the degree of mixing. In this Letter, we adopt $\eta = 0.1, 0.05$, and 0.01 to represent the degree of mixing from mild to weak.

By assuming the jet launching time as t_{launch}, the sweep-up mass M_{sw} from outflowing material in the jet can be described as

$$M_{\mathrm{jet}} \geqslant M_{\mathrm{sw}}(t_{\mathrm{launch}}) \equiv \int_0^{\theta_{\mathrm{ini}}} \eta M_{\mathrm{dyn}}(\theta) \sin \theta d\theta$$
$$+ 2\pi \int_0^{\theta_{\mathrm{ini}}} \int_{t_{\mathrm{dyn}}}^{t_{\mathrm{launch}}} \eta \dot{M}_{\mathrm{wind}}(\theta, t') \sin \theta dt' d\theta, \qquad (7)$$

where $t_{\mathrm{dyn}} \sim 10$ ms is the duration of tidal disruption, $t_{\mathrm{launch}} \geqslant t_{\mathrm{dyn}}$ is assumed, and the inequality in the beginning is introduced by involving the initial baryon loading of the jet during its launch. Here, $M_{\mathrm{dyn}}(\theta) = 3M_{\mathrm{dyn,tot}} \sin^2 \theta / (8\pi)$ describes the angle-dependent dynamic ejecta; $\dot{M}_{\mathrm{wind}}(\theta, t) = f\dot{M}_{\mathrm{NS}}(t) + 3\dot{M}_{\mathrm{disk}}(t) \sin^2 \theta / (8\pi)$ is the mass in the wind, $\dot{M}_{\mathrm{NS}}(t)$ is the quasi-isotropic NS-driven wind, and $\dot{M}_{\mathrm{disk}}(t)$ is the angle-dependent viscosity-driven disk wind. In our work, a uniform mass distribution within the polar angle $\theta_{\mathrm{neu}} \lesssim 60°$ for the NS-driven wind is adopted and thus $f = 4\pi / [2\pi(1 - \cos \theta_{\mathrm{neu}}) \times 2] = 2$ is introduced to describe the correction of mass distribution in the polar region for NS-driven wind. The different parts of $\dot{M}_{\mathrm{NS}}(t) = \dot{M}_{\nu,\mathrm{NS}}(t) + \dot{M}_{\mathrm{B,NS}}(t)$ and $\dot{M}_{\mathrm{disk}}(t) = \dot{M}_{\nu,\mathrm{disk}}(t) + \dot{M}_{\mathrm{B,disk}}(t)$, respectively, are given as (Gill et al. 2019)

$$\dot{M}_{\nu,\mathrm{NS}}(t) \approx \begin{cases} 1.13 \times 10^{-4} (t/1\ \mathrm{s})^{-0.98}, & t_{\mathrm{dyn}} < t < 0.2\ \mathrm{s}, \\ 2.02 \times 10^{-4} (t/1\ \mathrm{s})^{-0.62}, & t \geqslant 0.2\ \mathrm{s}, \end{cases} \qquad (8)$$
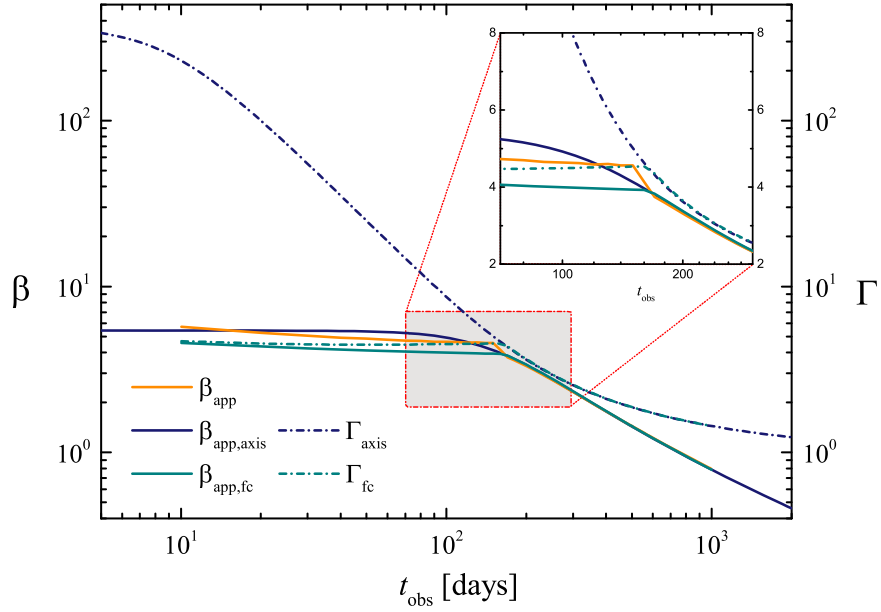
Figure 3. Dependence of β_{app}, $\beta_{app,axis}$, $\beta_{app,fc}$, Γ_{axis}, and Γ_{fc} on t_{obs}, where the meanings of lines are shown in the figure. The inset shows zoomed-in view of the period from 70 to 300 days.
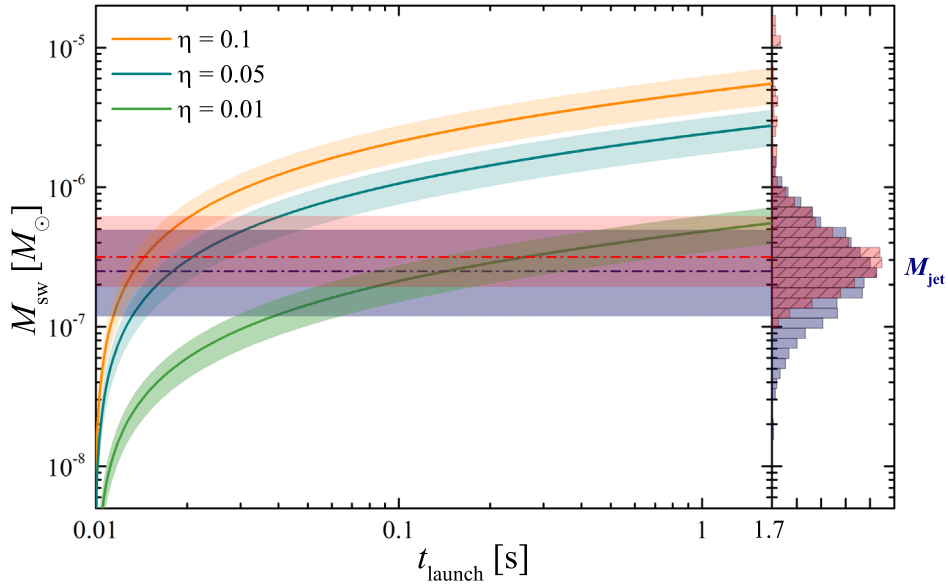
Figure 4. Dependence of M_{sw} on t_{launch} (left panel) and distribution of M_{jet} based on the MCMC samples (right panel). In the left panel, the yellow, blue, and green lines show the relations of $M_{sw}-t_{launch}$ with $\eta = 0.1, 0.05, 0.01$, respectively. In addition, the blue (red) dashed–dotted line shows the median values of M_{jet} by adopting power-law (Gaussian) structured jet in the fitting. The filled regions around lines display the corresponding 1σ uncertainties of M_{sw} or M_{jet}. In the right panel, the light-blue and light-red bars correspond to the case with power-law and Gaussian structured jet models, respectively.

$$\dot{M}_{B,NS}(t) \approx 5.18 \times 10^{-3}(t/1\ s)^{-0.9}, \qquad t \geqslant t_{dyn}, \qquad (9)$$

$$\dot{M}_{\nu,disk}(t) \approx \begin{cases} 1.43 \times 10^{-7}(t/1\ s)^{-2}, & t_{dyn} < t < 0.12\ s, \\ 1.22 \times 10^{-11}(t/1\ s)^{-6.4}, & t \geqslant 0.12\ s, \end{cases}$$
$$(10)$$

$$\dot{M}_{B,disk}(t) \approx 0.012, \qquad t \geqslant t_{dyn}, \qquad (11)$$

in units of $M_\odot\ s^{-1}$. The fractional uncertainties of Equations (8)–(11) are introduced in the same way as Gill et al. (2019). The

description of angle profile of the dynamic ejecta and viscosity-driven winds in Equation (7) are taken from Perego et al. (2017). In addition, a series of numerical simulations reported that the total mass of dynamic ejecta has $M_{dyn,tot} \sim 10^{-4}M_\odot-10^{-2}M_\odot$ (e.g., see Nakar 2019 for details) and $M_{dyn,tot} = (1.5 \pm 1.1) \times 10^{-3}M_\odot$ is adopted for our analysis (Gill et al. 2019). The initial jet-opening angle θ_{ini} cannot be known in advance and the MCMC fitting result $\theta_\varepsilon \sim 4°$ is adopted as a possible value of θ_{ini} in this work. The jet is assumed to be non-collimated by the outflows (Bromberg et al. 2011).

In Figure 4, we show the dependence of M_{sw} on t_{launch}, where different value of η, i.e., $\eta = 0.1, 0.05, 0.01$, are adopted. For a given M_{jet}, which is shown with the dashed–dotted line and the filled region in Figure 4, one can estimate the maximum value of t_{launch} by solving $M_{sw}(t_{launch}) = M_{jet}$. We note that the waiting time between the merger starting and the jet launching is less than 0.2 s if $\eta \gtrsim 0.01$ is taken. In addition, M_{jet} needs to increase by a factor of two (one magnitude) in order for the jet launching delay time to increase to around 1 s if $\eta = 0.01$ (0.05) is adopted. A higher η will lead to a lower waiting time for the jet launching. Note that the M_{sw} also depends on the initial opening angle θ_{ini}; a higher value of θ_{ini} means a lower upper limit of launching time as well.

4. Summary and Conclusion

In order to infer the baryon loading of the jet, we use a structured jet to fit the X-ray/optical/radio afterglows of GRB 170817A, together with the superluminal motion measurement of radio source in this burst. The structured jet is modeled with angle-dependent energy and baryon loading. The fitting result of the power-law structured jet shows that the ratio between the viewing angle and the jet core angle is $\theta_v/\theta_\varepsilon \sim 5$, which is consistent with other works utilizing the superluminal motion measurement in their fittings (Ghirlanda et al. 2019; Hotokezaka et al. 2019). The obtained θ_ε and θ_v are consistent with the results estimated based on the prompt emission of GRB 170817 (e.g., Mooley et al. 2018; Beniamini et al. 2019). The jet carries the total energy as a few times 10^{49} erg. The on-axis viewed isotropic energy is 10^{52}–10^{53} erg, which is relatively large but still reasonable (Mooley et al. 2018). The ISM number density is well below the upper limit on the density of the ionized and neutral particles $\sim 10^{-2}$ cm^{-3}. We also studied the motion of the flux centroid in the radio image. It should be noted that the behavior of the flux centroid is different for different jet structures and viewing angles.

Based on our fitting result, the baryon loading of the jet in GRB 170817A is inferred as $M_{jet} = 2.49^{+1.44}_{-1.30} \times 10^{-7} M_\odot$ ($M_{jet} = 3.16^{+2.04}_{-1.23} \times 10^{-7} M_\odot$) under the power-law (Gaussian) structured jet model. By comparing the baryon loading of the jet to the mass outflow in different ejecting stages, a conservative estimation reveals that the time lag of the jet launch relative to the merger is less than hundreds or tens of milliseconds. This result is consistent with the conclusion of Nagakura et al. (2014), which focused on the penetrability of jet in the merger outflow and confirmed a similar upper limit of the jet launch time with this work. Optimistic estimation would provide a lower upper limit of the jet launching time. Recently, works focused on the delay time between the merger and the jet launch of binary compact star merger have rich conclusions (e.g., Lazzati & Perna 2019; Beniamini et al. 2020a; Hamidani & Ioka 2020; Hamidani et al. 2020; Lazzati et al. 2020; Lyutikov 2020). These works are based on the dynamics of jet during its propagation in a presupposed isotropic-profile of outflows with or without expanding. Our discussion is based on a different method, and given an independent constraint. We notice that the uncertainties in our method mainly depend on the outflowing rate and angle profile of the merge outflows, and the fraction of outflowing material drawn into the jet. The angle profile of outflows may play an important role in the collimation of the jet and its breakout from the outflows. In addition, a successful jet launched by an NS may affect the mass of the outflow within the propagation path of the jet. Once
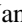
the mass of the outflow and/or the fraction of outflowing material drawn into the jet are well established, the launching time of a jet can be well constrained by utilizing the method proposed in this Letter. The numerical simulations of the propagation of the jet in the anisotropic and expanding outflows may be necessary in order to better understand the physics of outflows and jet formed in the merger (e.g., Murguia-Berthier et al. 2020).

The fate of the remnant of GW170817 event is still a mystery (e.g., Granot et al. 2017; Piro et al. 2019). As Beniamini et al. (2017, 2020a) have discussed, the high energy per baryon required for a jet launching delay of <0.1 s argues against a magnetar central engine for GRB 170817. Our fitting results of the power-law and the Gaussian structured jet seems to favor their opinion. However, the accretion of the disk to the NS may weaken the constraints of the jet launching time, because the energy released by accretion might be able to increase the energy per baryon (e.g., Zhang & Dai 2009, 2010; Metzger et al. 2018). Please see the discussion in Beniamini et al. (2020a).

ORCID iDs

Jia Ren ⓘ https://orcid.org/0000-0002-9037-8642
Da-Bin Lin ⓘ https://orcid.org/0000-0003-1474-293X
Lu-Lu Zhang ⓘ https://orcid.org/0000-0003-0726-7579
Xiang-Gao Wang ⓘ https://orcid.org/0000-0001-8411-8011
En-Wei Liang ⓘ https://orcid.org/0000-0002-7044-733X

References

Abbott, B. P., Abbott, R., Abbott, T. D., et al. 2017a, ApJL, 850, L39
Abbott, B. P., Abbott, R., Abbott, T. D., et al. 2017b, ApJL, 848, L13
Abbott, B. P., Abbott, R., Abbott, T. D., et al. 2017c, ApJL, 850, L40
Abbott, B. P., Abbott, R., Abbott, T. D., et al. 2017d, ApJ, 841, 89
Abbott, B. P., Abbott, R., Abbott, T. D., et al. 2017e, PhRvD, 96, 022001
Beniamini, P., Duran, R. B., Petropoulou, M., & Giannios, D. 2020a, ApJL, 895, L33
Beniamini, P., Giannios, D., & Metzger, B. D. 2017, MNRAS, 472, 3058
Beniamini, P., Granot, J., & Gill, R. 2020b, MNRAS, 493, 3521
Beniamini, P., Petropoulou, M., Barniol Duran, R., & Giannios, D. 2019, MNRAS, 483, 840
Beniamini, P., & van der Horst, A. J. 2017, MNRAS, 472, 3161
Bromberg, O., Nakar, E., Piran, T., & Sari, R. 2011, ApJ, 740, 100
Bromberg, O., Tchekhovskoy, A., Gottlieb, O., Nakar, E., & Piran, T. 2018, MNRAS, 475, 2971
Burns, E. 2019, arXiv:1909.06085
Connaughton, V., Burns, E., Goldstein, A., et al. 2016, ApJL, 826, L6
Connaughton, V., Burns, E., Goldstein, A., et al. 2018, ApJL, 853, L9
Coulter, D. A., Foley, R. J., Kilpatrick, C. D., et al. 2017, Sci, 358, 1556
Cowperthwaite, P. S., Berger, E., Villar, V. A., et al. 2017, ApJL, 848, L17
Fan, Y., & Piran, T. 2006, MNRAS, 369, 197
Fong, W., Blanchard, P. K., Alexander, K. D., et al. 2019, ApJL, 883, L1
Foreman-Mackey, D., Hogg, D. W., Lang, D., & Goodman, J. 2013, PASP, 125, 306
Ghirlanda, G., Salafia, O. S., Paragi, Z., et al. 2019, Sci, 363, 968
Gill, R., & Granot, J. 2018, MNRAS, 478, 4128

Gill, R., Nathanail, A., & Rezzolla, L. 2019, ApJ, 876, 139
Goldstein, A., Veres, P., Burns, E., et al. 2017, ApJL, 848, L14
Gottlieb, O., Bromberg, O., Singh, C. B., & Nakar, E. 2020a, MNRAS, in press
Gottlieb, O., Nakar, E., & Bromberg, O. 2020b, arXiv:2006.02466
Gottlieb, O., Nakar, E., Piran, T., & Hotokezaka, K. 2018, MNRAS, 479, 588
Granot, J., de Colle, F., & Ramirez-Ruiz, E. 2018, MNRAS, 481, 2711
Granot, J., Guetta, D., & Gill, R. 2017, ApJL, 850, L24
Greiner, J., Burgess, J. M., Savchenko, V., & Yu, H.-F. 2016, ApJL, 827, L38
Hajela, A., Margutti, R., Alexander, K. D., et al. 2019, ApJL, 886, L17
Hallinan, G., Corsi, A., Mooley, K. P., et al. 2017, Sci, 358, 1579
Hamidani, H., & Ioka, K. 2020, arXiv:2007.10690
Hamidani, H., Kiuchi, K., & Ioka, K. 2020, MNRAS, 491, 3192
Hotokezaka, K., Nakar, E., Gottlieb, O., et al. 2019, NatAs, 3, 940
Kasen, D., Metzger, B., Barnes, J., Quataert, E., & Ramirez-Ruiz, E. 2017, Natur, 551, 80
Kumar, P., Hernández, R. A., Bošnjak, Ž., & Barniol Duran, R. 2012, MNRAS, 427, L40
Lattimer, J. M., & Schramm, D. N. 1974, ApJL, 192, L145
Lattimer, J. M., & Schramm, D. N. 1976, ApJ, 210, 549
Lazzati, D., Ciolfi, R., & Perna, R. 2020, ApJ, 898, 59
Lazzati, D., & Perna, R. 2019, ApJ, 881, 89
Li, L.-X., & Paczyński, B. 1998, ApJL, 507, L59
Li, S.-Z., Liu, L.-D., Yu, Y.-W., & Zhang, B. 2018, ApJL, 861, L12
Lin, D.-B., Liu, T., Lin, J., et al. 2018, ApJ, 856, 90
Liu, K., Lin, D.-B., Wang, K., et al. 2020, ApJL, 893, L14
Lu, W., Beniamini, P., & McDowell, A. 2020, arXiv:2005.10313
Lyutikov, M. 2020, MNRAS, 491, 483
Makhathini, S., Mooley, K. P., Brightman, M., et al. 2020, arXiv:2006.02382
Matsumoto, T., Ioka, K., Kisaka, S., & Nakar, E. 2018, ApJ, 861, 55
Metzger, B. D. 2017, LRR, 20, 3
Metzger, B. D., Thompson, T. A., & Quataert, E. 2018, ApJ, 856, 101
Mooley, K. P., Deller, A. T., Gottlieb, O., et al. 2018, Natur, 561, 355
Murguia-Berthier, A., Ramirez-Ruiz, E., de Colle, F., et al. 2020, arXiv:2007.12245
Nagakura, H., Hotokezaka, K., Sekiguchi, Y., Shibata, M., & Ioka, K. 2014, ApJL, 784, L28
Nakar, E. 2019, arXiv:1912.05659
Nakar, E., & Piran, T. 2020, arXiv:2005.01754
Pe'er, A. 2012, ApJL, 752, L8
Perego, A., Radice, D., & Bernuzzi, S. 2017, ApJL, 850, L37
Piro, L., Troja, E., Zhang, B., et al. 2019, MNRAS, 483, 1912
Rees, M. J. 1966, Natur, 211, 468
Ren, J., Lin, D.-B., Zhang, L.-L., et al. 2019, ApJ, 885, 60
Ryan, G., Eerten, H. v., Piro, L., & Troja, E. 2020, ApJ, 896, 166
Sari, R., & Piran, T. 1999, ApJL, 517, L109
Sari, R., Piran, T., & Narayan, R. 1998, ApJL, 497, L17
Symbalisty, E., & Schramm, D. N. 1982, ApL, 22, 143
Troja, E., van Eerten, H., Ryan, G., et al. 2019, MNRAS, 489, 1919
Villar, V. A., Guillochon, J., Berger, E., et al. 2017, ApJL, 851, L21
Waxman, E., Ofek, E. O., Kushnir, D., & Gal-Yam, A. 2018, MNRAS, 481, 3423
Yang, Y.-S., Zhong, S.-Q., Zhang, B.-B., et al. 2020, ApJ, 899, 60
Yu, Y.-W., Liu, L.-D., & Dai, Z.-G. 2018, ApJ, 861, 114
Zhang, B. 2018, The Physics of Gamma-Ray Bursts (Cambridge: Cambridge Univ. Press)
Zhang, B. 2019, FrPhy, 14, 64402
Zhang, B.-B., Zhang, B., Sun, H., et al. 2018, NatCo, 9, 447
Zhang, D., & Dai, Z. G. 2009, ApJ, 703, 461
Zhang, D., & Dai, Z. G. 2010, ApJ, 718, 841
Zhu, J.-P., Yang, Y.-P., Liu, L.-D., et al. 2020, ApJ, 897, 20